blood advances

American Society of Hematology
2021 L Street NW, Suite 900,
Washington, DC 20036
Phone: 202-776-0544 | Fax 202-776-0545
bloodadvances@hematology.org

CD20 Bispecific T cell Engager Depletes B Cell Progenitors Preventing EBV-Associated Lymphomagenesis in Humanized Mice

Tracking no: ADV-2025-019375R1

Michelle Böni (University of Zurich, Switzerland) Patrick Schumachers (University of Zurich, Switzerland) Saskia von Boxberg (University of Zurich, Switzerland) Amanda Poon (University of Zurich, Switzerland) Emeline Thevenon (Novartis, Switzerland) Daniele Mennonna (Novartis, Switzerland) Melissa Ramones (Novartis, United States) Lucas Romann (University of Zurich, Switzerland) Svenja Walter (University of Zurich, Switzerland) Eanna Fennell (University of Zurich, Switzerland) Francesca Rucci (Novartis, Switzerland) Elisabetta Traggiai (Novartis, Switzerland) Christian Münz (University of Zurich, Switzerland)

Abstract:
Epstein Barr virus (EBV) infection is associated with around 1.5% of human tumors, including B cell lymphoproliferative diseases (LPD). A common approach in treating EBV-associated LPDs is targeting infected tumor cells with a CD20 monoclonal antibody, such as Rituximab, although this often fails to prevent relapse and refractory disease. In this study, we show in a pre-clinical humanized mouse model superior efficacy of a CD3xCD20 bispecific T cell engager (CD20 TCE) in preventing systemic virus spread and EBV-associated tumor formation as compared to Rituximab treatment. Increased efficacy is associated with a deep depletion of human precursor B cells in the bone marrow. Progenitor B cells are permissive to infection with EBV in vitro and correlate with EBV persistence during B cell depletion therapy also in vivo. Thus, deep depletion of B cells including bone marrow progenitors might target EBV-associated LPDs more efficiently and infected progenitors should be considered as an EBV reservoir from which associated pathologies could relapse.

Conflict of interest: No COI declared

COI notes:

Preprint server: No;

Author contributions and disclosures: Conceptualization: MB, PS, CM; Methodology: MB, PS; Formal analysis: MB, PS, EF; Investigation: MB, PS, AP, ET, MR, DM, SvB, LR, SW; Resources: FR, ET, CM; Data Curation: MB, PS; Writing-original draft preparation: MB, PS; Writing-review and editing: MB, PS, CM; Visualization: MB, PS; Supervision: CM, FR, ET; Project administration: MB, PS; Funding acquisition: MB, CM, FR, ET.

Non-author contributions and disclosures: No;

Agreement to Share Publication-Related Data and Data Sharing Statement: The previously deposited datasets of NCBI GEO GSE299939 and GSE2533555 were used for some analyses in the manuscript and are referenced.

Clinical trial registration information (if any):

CD20 Bispecific T cell Engager Depletes B Cell Progenitors Preventing EBV-Associated Lymphomagenesis in Humanized Mice

Michelle Böni[1], Patrick Schuhmachers[1*], Saskia von Boxberg[1], Amanda Poon[1,2], Emeline Thevenon[3], Daniele Mennonna[3], Melissa Ramones[4], Lucas Romann[1], Svenja L. Walter[1], Éanna Fennell[1,5], Francesca Rucci[3], Elisabetta Traggiai[3], Christian Münz[1#]*

**Authors contributed equally to this work*

[#]Corresponding author christian.muenz@uzh.ch,

Affiliations

[1]Viral Immunobiology, Institute of Experimental Immunology, University of Zurich, Switzerland

[2]Present address: Creoptix AG, Wädenswil, Switzerland

[3]Novartis Biomedical Research, Basel, Switzerland

[4]Novartis Biomedical Research, Cambridge, Massachusetts, United States of America [5]School of Medicine, Bernal Institute, Health Research Institute, Limerick Digital Cancer Research Centre, University of Limerick, Limerick, Ireland.

Key Points

- *CD3xCD20 bispecific TCE depletes precursor B cells in primary lymphoid organs.*
- *Depletion of B cell precursors permissive to EBV infection is associated with more effective prevention of EBV-associated lymphomagenesis, surpassing the efficacy of Rituximab.*

Data Sharing Statement

- *For original data, please contact christian.muenz@uzh.ch*

Manuscript length restrictions

- *Text word count: 4259*
- *Abstract word count: 157*
- *Number of figures: 5*
- *Number of references: 69*

Abstract

Epstein Barr virus (EBV) infection is associated with around 1.5% of human tumors, including B cell lymphoproliferative diseases (LPD). A common approach in treating EBV-associated LPDs is targeting infected tumor cells with a CD20 monoclonal antibody, such as Rituximab, although this often fails to prevent relapses and refractory disease. In this study, we show in a pre-clinical humanized mouse model superior efficacy of a CD3xCD20 bispecific T cell engager (CD20 TCE) in preventing systemic virus spread and EBV-associated tumor formation as compared to Rituximab treatment. Increased efficacy is associated with a deep depletion of human precursor B cells in the bone marrow. Progenitor B cells are permissive to infection with EBV *in vitro* and correlate with EBV persistence during B cell depletion therapy also *in vivo.* Thus, deep depletion of B cells including bone marrow progenitors might target EBV-associated LPDs more efficiently. Infected progenitors should be considered as an EBV reservoir from which associated pathologies could relapse.

Introduction

More than 90% of adults are persistently infected with the Epstein-Barr virus (EBV) without developing EBV-associated disease[1]. Nevertheless, EBV is a WHO class I carcinogen responsible for around 1.5% of cancers[2,3]. EBV-associated cancers derive directly from infected cells and include carcinomas and lymphoproliferative diseases (LPDs), especially of B cell origin[2,4]. *In vitro,* EBV efficiently infects B cells and immortalizes them into continuously proliferating lymphoblastoid cell lines (LCL)[5]. *In vivo*, however, EBV persists in resting memory B cells, an alleged contradiction explained by the germinal center (GC) model of EBV persistence[6,7]. In this model, EBV is thought to cross the oropharyngeal epithelium to infect naïve B cells through interactions between viral glycoproteins with receptors such as CD21, CD35, MHC class II, α_v integrins, ephrin type-A receptor 2, neuropilin-1 and regulator of G protein signaling 9 binding protein (R9AP)[8–14]. Infection activates B cells, inducing differentiation into proliferating blasts undergoing a GC-like reaction, ultimately generating resting memory B cells. Upon terminal plasma cell differentiation, these may release infectious virions. During primary infection, infected B cells accumulate and circulate until adaptive immunity reduces viral loads through massive T cell activation and expansion. This T cell response spares latently infected memory B cells, allowing EBV persistence as an ongoing cycle of infection, differentiation, persistence, reactivation and reinfection without being oncogenic by default in the healthy host.

Each step within this lifecycle exhibits characteristic EBV latency programs[15]. EBV-associated B cell malignancies likely arise from the combined events of EBV oncogene expression, GC-associated mutagenesis, and cell cycle dysregulation during EBV-driven B cell differentiation, explaining the presence of all latency programs in EBV associated LPDs[2,15]. These disorders are therefore highly heterogeneous in pathogenesis and B cell developmental stages, requiring tailored therapies. Yet, their mostly shared B cell origin renders them susceptible to CD20-targeting antibodies. Rituximab, a monospecific CD20 antibody, is part of chemotherapy schemes for EBV-associated LPDs such as diffuse large B cell and Burkitt lymphoma, and is first-line therapy for posttransplant lymphoproliferative disorders (PTLD)[16–19]. PTLD response rates to Rituximab exceed 70%, but mortality surpasses 90% in non-responders[20]. Alternative treatments include CD19 CAR T cells or autologous EBV-specific T cells[17].

Recently, T cell engaging antibodies (TCE) have advanced lymphoma therapy[21–23]. By co-binding CD3 on T cells and tumour associated antigens, TCE recruit and activate potent cytotoxic T cells to eliminate tumor cells independently of native T cell receptor specificity, achieving greater depletion efficacy than monoclonal antibodies[21]. As “off-the-shelf” therapies, they offer superior availability and logistical practicality compared to CAR or EBV-specific T cell therapies[17]. However, their effects on EBV-induced lymphoma and viral persistence remain poorly characterized. In this study, we investigated a CD3xCD20 bispecific TCE in EBV-infected mice with reconstituted human immune systems (humanized mice).

Compared to monospecific anti-CD20 therapy, we observed better prevention of EBV-associated tumor formation and reduced virus dissemination. This was associated with enhanced B cell depletion across primary and secondary lymphoid organs and across a broader range of B cell developmental stages, including precursor B cells permissive to EBV infection. This might indicate relevance of precursor B cells in EBV persistence during the self-perpetuating cycle of infection, differentiation, persistence, reactivation and reinfection in the setting of B cell depletion therapies.

Methods

Ethics statement

All animal experiments as well as the use of peripheral blood mononuclear cells (PBMCs) from human donors followed the protocols in licenses ZH042/2021, ZH074/2024, or KEK-ZH-Nr. 2010-0057 and 2019-00837. This study was conducted in accordance with the Declaration of Helsinki.

Humanized mouse generation

Newborn NOD.Cg-Prkdc^{scid}Il2rg^{tm1Wjl}/SzJ (Strain #005557, NSG), NOD.Cg-Rag1^{tm1Mom}Flt3^{tm1Irl}Mcph1$^{Tg(HLA-\ A2.1)1Enge}$Il2rg^{tm1Wjl}/J (Strain #033127, NFA2, for experiments depicted in Fig. 5I, S3D) or BRGS-A2DR2 (provided by Regeneron, for experiment 5G) pups, one to five days of age, were sublethally irradiated with 1Gy and intrahepatically injected with 1-3x10^5 human fetal liver (HFL) derived (Advanced Bioscience Resources, Cercle Allocation Services, Inc.) CD34$^+$ hematopoietic progenitor cells (HPCs). Only animals with >10% huCD45$^+$ cells of all leukocytes after three months and animals with a reconstituted T cell compartment were included in the experiments. Details of HPC-isolation and randomization are provided in supplemental methods.

CD3xCD20 TCE Design

TheCD3ε binding moiety of the CD3xCD20 TCE used for the experiemts consists of a humanized single chain antibody (scFv) that was derived from the mouse anti CD3 antibody SP34 while the CD20 binding arm consists of a Fab corresponding to Rituximab. Hetero-dimerization of the Fc was achieved by the 'knobs-into-holes' engineering[24]. Constant human IgG1 Fc sequence contained modifications that silence antibody dependent cellular cytotoxicity and facilitate purification of heterodimeric Fc multi-specific antibodies while retaining binding to FcRn. Details for the CD3xCD20 TCE production are provided in supplemental methods.

Virus Infection and Antibody Treatment of Humanized Mice

Three to six months old humanized mice were intraperitoneally injected with 10^5 Raji infectious units (RIU) of recombinant EBV B95-8 or mock infected with PBS. Starting two weeks after EBV infection, animals were intraperitoneally injected with 0.1mg/kg CD20 TCE, 0.1mg/kg isotype control, 10mg/kg Rituximab (Mab Thera, Roche Pharma), the vehicle only or with PBS. Antibody injections were repeated weekly. The last injection occurred seven days before the experimental endpoint. Animals were euthanized five weeks post infection by CO_2 inhalation or if predetermined humane endpoints were met as defined in the animal licenses. Details on EBV production and animal housing conditions are provided in supplemental methods.

Cell Analysis

Splenocytes, bone marrow and PBMC cells were isolated from humanized Mice and stained for flow cytometry analysis. For downstream UMAP visualizations and high dimensional analysis, the Cyclone R-based Pipeline available on GitHub was used [25]. Additionally, DNA was extracted from isolated cells and the EBV BamH-I W fragment was measured via qPCR to assess viral loads. Plasma and serum samples were analyzed for cytokines using an MSD V-Plex assay (mesoscale) and for immunoglobulins using a Bio-Plex Assay (Bio Rad). Tumor formation was assessed macroscopically and EBV presence in tumors was confirmed by immunohistochemical stainings for nuclear antigen 2 of EBV (EBNA2) of paraffin-embedded slides. Details about individual assays are described in the supplemental methods.

Precursor B cell Infection

$CD24^+$ precursor B cells were isolated via fluorescent activated cell sorting (FACS) and infected with EBV B95-8 or M81 with an MOI1. RNA was isolated 72h post-infection and analyzed via qRT-PCR for EBV gene expression or cells were co-stained 72h post-infection for nuclear EBNA1 and CD24 and analyzed by Image Stream X Mark II. Alternatively, B cells were isolated via FACS from EBV-infected huMice and sorted fractions were analyzed for EBV infection by qPCR for EBV BamHI-W fragments. Additional details are provided in the supplemental methods.

Results

CD20 bispecific T cell engager-mediated B cell depletion prevents systemic virus spread and EBV-induced tumor formation

Humanized NOD.Cg-Prkdc^{scid} Il2rg^{tm1Wjl}/SzJ (huNSG) mice infected with EBV were previously shown to establish a latent infection[26,27]. Although virus-specific T cell responses are induced in response to the infection, formation of EBV-associated lymphomagenesis was reported[26]. To investigate the efficacy of a CD3xCD20 bispecific T cell engager (CD20 TCE) on EBV-associated lymphomagenesis, we infected huNSG mice with EBV wild-type (EBVwt, B95-8). After allowing EBV to establish a latent infection for two weeks, animals received three doses of CD20 TCE on a weekly basis. Animals were euthanized at five weeks post-infection or if predetermined humane endpoints were met (**Fig. 1A**). Even with the high inter-mouse variability typical of humanized models, CD19$^+$ and CD20$^+$ B cell numbers in peripheral tail vein blood declined noticeably as early as six hours after the first antibody dose and continued to decrease over time (**Fig. 1B, Fig. S1A**). This decrease was not attributed to competitive binding of the CD20 TCE and the detection antibody for CD20 (**Fig. S1B**). Likewise, CD19$^+$ and CD20$^+$ B cell were depleted in primary and secondary lymphoid organs such as bone marrow (BM) and spleen, both reservoirs of memory B cells, the site of long-term EBV persistence[6,28] (**Fig. 1C, Fig. S1C**). Accordingly, EBV-infected and CD20 TCE treated animals had no detectable viral loads in the blood over the whole course of the experiment, while viral presence was still detectable in the spleen of a minority of animals (**Fig. 1D-E)**. Yet, none of the EBV-infected and CD20 TCE treated animals developed lymphomas during the experiment whereas lymphomas occurred in ≥50% of animals receiving either the isotype control (TCE with anti-growth hormone binding arm) or vehicle alone (buffer used to dissolve the TCE) (**Fig. 1F**). We conclude that despite cases of only partial responses, CD20 TCE treatment effectively prevents systemic virus spread in blood as well as EBV-induced lymphomagenesis in humanized mice.

T cells expand and differentiate after CD20 TCE injection

T cell redirecting therapies can commonly lead to a cytokine release syndrome (CRS) due to extensive T cell engagement[29,30]. EBV is a strong driver of T cell proliferation itself and induces this phenotype also in EBV-infected humanized mice[26,31]. To avoid hyperactivation of EBV-induced and expanded T cells by injection of the CD20 TCE, we started with treatment injections two weeks after EBV infection, when EBV-specific immune responses had been primed but prior to EBV-induced T cell proliferation. Nevertheless, we clinically observed a substantial weight loss in treated animals after the first dose of CD20 TCE, followed by a complete recovery during the remaining experiment (**Fig. 2A**). This weight loss was dose-dependent and led to premature euthanasia of individual mice (**Fig. S2A-C**). The observed weight loss was accompanied by a strong increase in plasma pro-inflammatory cytokine levels six hours after the first TCE injection (IFN-γ, IL-1β, TNFα, IL-2, IL-4, IL-6, IL-8, IL-10, IL-12p70

and IL-13) (**Fig. 2B**). EBV infection had no influence on the amount of cytokines released at that time point (**Fig. S2D**). Furthermore, we did not see any association between the magnitude of the cytokine release in week two and systemic virus spread at the end of the experiment (data not shown). Consistent with previous reports on T cell margination and extravasation induced by the cytokine release, we also observed a significant reduction in the numbers of peripheral blood $CD3^+$, mainly $CD8^+$ T cells, six hours after the first TCE injection (**Fig. 2C, S3A-C**)[32–34]. This was followed by a massive expansion in week three and subsequent contraction to levels lower than in EBV-infected control groups. Since viral loads were not observed in blood after treatment, strong EBV-driven T cell expansion, potentially requiring high amounts of antigens, was not observed in CD20 TCE treated animals. Nonetheless, EBV-specific T cells were detectable at endpoint by IFNγ ELISPOT in a preliminary assay, indicating that CD20-directed TCE treatment does not prevent the development of EBV-specific effector or memory T cells (**Fig. S3D**). Also, there was no association between T cell margination and systemic virus spread (**Fig. S3E**). However, we did see a stronger $CD8^+$ T cell activation six hours post first TCE dose in animals with suppressed viral loads (**Fig. S3F**). Treatment with the CD20 TCE led to an increase in the proportion of activated T cells as measured by HLA-DR and PD-1 six hours after TCE injection in week two and stayed high during the remaining course of the experiment. Unactivated T cells started to decline in EBV-infected control groups only in week 4 (**Fig. 2D-E, Fig. S4A-B**). Simultaneously, EBV infection was driving T cells into a $CD45RA^-CCR7^-$ effector memory differentiation (**Fig. 2F).** Similarly, CD20 TCE treatment induced an effector memory phenotype after administration of the first dose but also led to a strong increase in $CD45RA^+CCR7^-$ Temra cells over time (**Fig. 2F-G, Fig. S4C-D**). In summary, EBV-infected CD20 TCE treated animals recapitulate similar uncontrolled immune activation as observed in CD20 TCE treated patients. While associations of biomarkers corresponding with remission in lymphoma patients such as increased T cell margination were not correlating with EBV control in humanized mice, activation of $CD8^+$ T cells after the first antibody injection did[33,34].

CD20 TCE treatment prevents EBV-induced lymphomagenesis more efficiently than the CD20 monospecific antibody Rituximab

Rituximab, a CD20 monospecific antibody, is an integral part of treatment regimens for EBV-associated lymphoproliferative diseases but only achieves a partial depletion of B cells in the bone marrow[35–38]. Having observed an almost complete B cell depletion upon CD20 TCE treatment, we investigated if control of viral infection by this treatment was more efficient than Rituximab administration. To that end, EBV-infected humanized mice were either treated with three doses of Rituximab or the CD20 TCE on a weekly basis. Animals received a molar dose of Rituximab exceeding that of the CD20 TCE by more than 20-fold, which was well tolerated (**Fig. S5A**). Infected isotype treated animals as well as PBS mock infected animals served as controls (**Fig. 3A**). Peripheral blood $CD19^+$ and $CD20^+$ B cells were effectively depleted upon mono- and bispecific antibody treatment, with a tendency to a better

depletion of $CD19^+$ B cells in CD20 TCE treated animals (**Fig. 3B**). Higher frequencies of $CD19^+$ and $CD20^+$ B cells in CD20 TCE treated animals in week two can be explained by the concomitant reduction in T cell numbers (**Fig. 2C**). The same tendency towards a better depletion of B cells by the CD20 TCE compared with Rituximab was observed in the spleen and bone marrow, with particularly pronounced reductions of $CD19^+$ B cells in the bone marrow (**Fig. 3C**). A stark difference in peripheral blood viral load suppression was observed between the two antibody regimens. Rituximab-treated animals predominantly exhibited high peripheral blood viral loads, comparable to those in isotype control animals; in contrast, EBV loads remained suppressed throughout the experimental period in all CD20 TCE-treated animals with the exception of a single subject (**Fig. 3D**). Splenic EBV loads were also reduced in CD20 TCE-treated animals relative to those receiving Rituximab. Nevertheless, a subset of mice remained EBV-positive in the spleen and bone marrow after treatment with the CD20 TCE (**Fig. 3E**). Despite measurable viral loads in lymphoid organs, CD20 TCE-treated animals remained free of tumors while almost 50% of the animals developed tumors under Rituximab treatment (**Fig. 3F**). Consistent with ongoing virus replication in the Rituximab cohort, T cell activation and differentiation kinetics in Rituximab-treated animals mirrored those observed in EBV-infected isotype-treated control animals (**Fig. S5B-E**). We therefore conclude that TCE treatment is more effective at preventing EBV-associated lymphomagenesis than monospecific antibody treatment with Rituximab.

CD20 TCE treatment depletes precursor B cells in the bone marrow

In order to understand if virus spread in monospecific antibody but not TCE-treated animals occurs because of protected B cell niches not targeted by Rituximab, we compared the phenotype of residual B cells at the end of the experiment in blood, spleen and bone marrow across both treatment groups. After manual gating of flow cytometry data from one experiment on human $CD45^+$ $CD19^+$ and/or $CD20^+$ B cells, we performed FlowSOM clustering as well as dimensionality reduction and visualization using uniform manifold approximation and projection (UMAP, **Fig. 4A**). Based on the different marker expression, we coarsely distinguished between $CD24^+$ precursor, transitional, naïve, IgD/CD27 double negative and switched memory B cells (**Fig. 4B, Fig S6A**). UMAP visualization of the different treatment groups showed a reduction in abundance and in the spectrum of B cell phenotypes in the CD20 TCE-treated cohort and a selective decrease in naïve B cells in the Rituximab-treated group, indicating a broader range of B cell depletion upon CD20 TCE treatment (**Fig. 4C**). B cell subset frequencies in untreated PBS animals differed between the organs (**Fig. 4D**). While $CD24^+$ precursor B cells make up the majority of B cells in the bone marrow, further differentiated cells like transitional, naïve and some double negative cells can be found in the periphery. EBV infection itself appears to promote the development of switched memory B cells, as confirmed by manual gating in two independent experiments, which showed a trend towards higher memory B cell frequencies in isotype-treated animals compared with PBS

mock-infected controls (**Fig.4E, Fig. S6B-C**). Consistent with this, EBV-infected animals showed increased levels of soluble IgG3 relative to PBS mock-infected animals, in line with RNA-seq data reporting an enrichment of IghG3 transcripts during EBV infection (**Fig. S6D**,[39]). The B cell composition in the bone marrow of Rituximab treated animals did not differ from control animals, but there was a strong reduction of naïve B cells in the periphery and $CD24^+$ precursor cells were enriched in the spleen, as confirmed by manual gating (**Fig. 4D-E**). While CD20 TCE treated animals were also depleted of naïve B cells, they additionally lacked $CD24^+$ precursor B cells in the bone marrow as well as transitional B cells in the periphery. In line with these findings, soluble IgM was reduced in TCE treated animals (**Fig. S6D**). Consequently, those mice presented predominantly with further differentiated B cell populations, including switched memory and double negative B cells, but still at markedly lower numbers than in untreated animals (**Fig. S6C**). This is of interest, because most of the $CD24^+$ precursor B cells are $CD20^{dim}$ (**Fig. 4B**) and are still targeted by the CD20 TCE while they are not affected by Rituximab.

Depletion of precursor B cells may protect from systemic virus spread

To determine whether $CD24^+$ precursor B cells might contribute to increased viral loads, we performed UMAP analysis plotting bone marrow, spleen and blood cells from CD20 TCE treated animals stratified by EBV viral load detectability in any organ via BamHI W fragment specific qPCR (responders and non-responders). Indeed, animals with detectable viral DNA (non-responders) exhibited an increased density of $CD24^+CD38^+CD10^+$ precursor B cells similar to the profile observed in Rituximab-treated animals (**Fig. 5A**). A higher frequency of $CD24^+$ precursor B cells in CD20 TCE-treated animals with detectable viral DNA was also confirmed by manual gating (**Fig 5B**). Furthermore, $CD24^+$ precursor B cells were also the only subset that was enriched in frequency in all treated animals (Rituximab and TCE) in non-responders compared to responders (**Fig. S7A**). *In vivo*, EBV persists in memory B cells and it is therefore rather unlikely, that precursor B cells might be a site for persistence. Hence, they might rather play a role early in infection which is why we tested, if $CD24^+$ precursor B cells are susceptible to EBV infection. We isolated splenocytes and bone marrow cells from naïve uninfected humanized mice and sorted $CD24^+$ and $CD24^-$ B cell fractions by fluorescence activated cell sorting (FACS) (**Fig. S7B**). From the bone marrow cells, $CD24^+$ but not $CD24^-$ fractions could be sorted in numbers that allowed to perform an infection assay. Directly after sorting, cells were infected with EBV at an MOI of 1. 72 hours post-infection, RNA was isolated and analyzed for EBV transcripts or co-expression of EBNA1 and CD24 was analyzed with the Image stream indicating successful infection of the B cells (**Fig. 5C**). EBV transcripts for EBNA2, LMP1, LMP2A and BZLF1 were detected in $CD24^+$ B cell fractions from both, spleen and bone marrow (**Fig. 5D**). These $CD24^+$ cells exhibited infection levels similar to the $CD24^-$ fraction from the spleen, which includes canonical targets for EBV infection such as naïve and memory B cells, despite low expression of established EBV entry receptors such as CD21 or CD35 (**Fig. 5E, Fig. S7C**). To exclude residual $CD24^-$ cell contamination after FACS sorting as a source of qPCR signal, additional ImageStream analysis was performed, demonstrating nuclear EBNA1 expression within $CD24^+$ B cells and thereby confirming their direct infection (**Fig. 5F-G, Fig.**

S8A). To extend our findings of CD24$^+$ B cell infection by EBV beyond the B95-8 virus strain, the ImageStream validation was also performed with rM81 EBV and yielded similar results. To assess precursor B cell infection *in vivo*, we FACS-sorted CD24$^+$ and CD24$^-$ B cells from the bone marrow of EBV-infected humanized mice (**Fig. 5H, Fig. S7B**). We detected an enrichment of BamHI-W fragments in CD24$^+$ precursor B cells relative to the unsorted population in 4 out of 7 mice, though the signal was in general lower than in CD24$^-$ B cells (**Fig. 5I**). Infection of precursor B cells was further supported by single cell RNA sequencing (scRNAseq) data generated from splenocyte-derived B cells of EBV infected humanized mice (**Fig. S8B**)[39]. We therefore propose that CD24$^+$ precursor B cells can be a potential target of EBV infection which might become relevant under B cell-depleting conditions, and that the extent of CD24$^+$ precursor B cells depletion correlates with the efficacy of B cell depletion therapy on EBV infection.

Discussion

In this study, we investigated the efficacy of a CD3xCD20 bispecific TCE on EBV persistence and EBV-associated tumor formation in a preclinical *in vivo* model. CD20 TCE treatment efficiently protected from lymphomagenesis and systemic virus spread, outperforming monospecific antibody treatment with Rituximab. This higher efficacy was associated with a more rigorous depletion of $CD20^+$ and $CD19^+$ B cells in blood, spleen and bone marrow, reflecting higher activity in secondary lymphoid organs. In patients, a single dose of Rituximab effectively depletes circulating B cells while immature and transitional B cells persist the bone marrow, and lymph nodes and spleens partially retain $CD20^-$ plasma cells and $CD27^+$ memory B cells[36–38,40,41]. Our preclinical *in vivo* model recapitulated these features of an near-complete peripheral depletion, partial splenic depletion with residual memory B cells and an intact B cell precursor compartment in the bone marrow, despite primarily early differentiated natural killer (NK) cell reconstitution and complement C5 deficiency in humanized NSG mice, diminishing antibody dependent cellular cytotoxicity (ADCC) and complement activation[42,43]. However, it has already previously been shown that Rituximab opsonized B cell lymphoma cells can be depleted in humanized NSG mice[43]. Furthermore, several other human immune system compartments were depleted in humanized mice by Fc receptor engaging antibodies, including classical and plasmacytoid dendritic cells, NK cells, $CD4^+$ and $CD8^+$ T cells, most likely due to antibody dependent cellular phagocytosis (ADCP)[44–46]. Accordingly, and similar to patients, Rituximab reduced lymphoma incidence in EBV infected humanized mice. However, CD20 TCE completely abolished lymphoma incidence and, surprisingly, depleted precursor B cells. CD20 expression is induced only in late pre-B cells and also in our flow cytometry data the majority of precursor B cells in the bone marrow of humanized mice was negative for CD20 [47]. In patients, transient cytopenia is a common adverse effect of bispecific TCEs[48,49]. While the underlying mechanism is unclear, a bystander effect of cytokine-mediated suppression of hematopoiesis is suspected. Partially supporting this, we observed that an increased T cell activation, though not elevated cytokine release, after the first TCE injection was associated with stronger depletion of precursor B cells.

CD20 TCE treated animals were also depleted of a broader range of different developmental B cell stages. The few remaining cells were mainly differentiated $CD27^-IgD^-$ or $CD27^+$ switched memory cells, the known site of EBV latency. Surprisingly, their frequency and number did not differ between animals with or without detectable viral loads, nor between monospecific and TCE-treated animals. In contrast, $CD24^+$ precursor B cells were enriched in depleted animals with detectable viral loads and therefore associated with systemic virus spread and lymphomagenesis. Current models of EBV's life cycle postulate direct infection of memory cells or infection of naïve B cells with EBV driving their differentiation into memory cells[15]. Precursor B cells, expressing canonical EBV entry receptors CD21 and CD35 only at low levels, are not part of this model. Nevertheless, we could show that precursor B cells from adult human bone marrow can be infected with EBV *in vitro*, in agreement with previous

findings using fetal bone marrow derived cells[50–52]. Public scRNA-seq datasets of human bone marrow confirmed low expression of CD21, CD35 or EphA2, but indicated the expression of integrin α_v and β1 on precursor B cells, which might mediate EBV entry[53]. Although the causal involvement of precursor B cells in the EBV life cycle *in vivo* remains unclear, the detection of precursor B cells among 0.2% of infected splenocytes in untreated EBV-infected humanized mice by scRNA-seq indicates that these cells can be infected *in vivo*. It is noteworthy that precursor cells are present in low frequencies in spleens of untreated EBV-infected animals, particularly five weeks post-infection when scRNA-seq was performed, indicating that reinfection occurs during EBV life cycle in humanized mice, as infected cells are unlikely to remain inactive and undifferentiated for such a duration. In summary, we provide evidence that under B cell depletion, when conventional targets of EBV infection are scarce, precursor B cells might become increasingly relevant. They might be susceptible to reinfection and sustain the ongoing cycle of infection, differentiation, persistence, and reactivation during EBV persistence.

Beyond providing insight into EBV biology, our data support consideration of bispecific TCEs as an alternative line of therapy for EBV-associated B cell LPDs. While these therapies carry a heightened risk of substantial toxicities due to immune activation and CRS, there is a consensus to date on best practices for managing and reducing CRS, such as corticosteroid premedication, step-up dosing, or preemptive administration of CD20 monoclonal antibodies[54,55]. Although not tested here, we assume that such interventions would not alter the outcome, as previous studies have shown that CRS mitigation does not diminish antitumor activity, as the CRS appears dispensable for effective T cell antitumor responses[32,55]. In addition to CRS, heightened susceptibility to fungal, viral and primarily bacterial infections are of concern during B cell depleting therapies and require sometimes adoptive transfer of intravenous immunoglobulins (IVIG) from healthy donors to restore pathogen specific antibody titers[56]. As a next step, CD3xCD19 TCEs in EBV-associated LPDs should be systematically explored, particularly in cases where Rituximab fails due to CD20-negative tumor cells. Successful use of CD3xCD19 bispecific TCE has already been reported in individual patients[57,58]. Given CD19 expression on earlier B cell stages, including precursors lacking CD20 expression, CD19-targeting approaches might be of particular interest if these cells indeed contribute to EBV persistence. Alternatively, direct targeting of CD24 could complement CD20-targeted B cell depletion. Our study therefore identifies precursor B cells as targets of EBV infection and persistence during CD20 targeted depletion treatments for LPDs.

Acknowledgements

We would like to thank Kristin Mansee for the maintenance of the humanized mice at the University of Zurich, Petra Hirschmann and Obinna Chijioke (Pathology University Hospital Basel) for the immunohistochemical stainings of the tissue sections, the cytometry facility (University of Zurich) for providing guidance with the FACS sorting, Amy Rayo and Kimberly Aardalen (Novartis) for the serum analysis, Brian Granda (Novartis) for resource support, and Lukas Egli, Fabienne Läderach, Yueyan Liao, Juliane Mietz, Maria Pena-Francesch, Arianna Picozzi, Lisa Rieble, Sandra Schmid, Alma Delia Valencia Camargo (Institute of Experimental Immunology, University of Zurich) for helping processing the animals at study endpoints. This research was supported by the Swiss National Science Foundation (3200-0-239903, 310030E_238141 and CRSII_222718_10000065), Swiss Cancer League (KFS-5896-08-2023-R), the Swiss MS Society (2023-17), the Swiss State Secretariat for Education, Research and Innovation (SERI) for EU Horizon BEHIND-MS (101137235), CRPP-ImmunoCure of the University of Zürich, the Sobek Foundation, the Swiss Vaccine Research Institute, the Vontobel Foundation, Roche, Novartis, Pfizer and Viracta to C.M. M.B. was supported by an MD-PhD fellowship from the Swiss Academy of Medical Sciences, Switzerland (323630_19938).

Authorship Contributions

Conceptualization: MB, PS, CM; Methodology: MB, PS; Formal analysis: MB, PS, EF, SvB; Investigation: MB, PS, AP, ET, MR, DM, SvB, LR, SW; Resources: FR, ET, CM; Data Curation: MB, PS; Writing-original draft preparation: MB, PS; Writing-review and editing: MB, PS, CM; Visualization: MB, PS; Supervision: CM, FR, ET; Project administration: MB, PS; Funding acquisition: MB, CM, FR, ET.

Conflicts of Interest

The authors declare no conflict of interest.

References

1. Cesarman E. Gammaherpesviruses and Lymphoproliferative Disorders. *Annu Rev Pathology Mech Dis*. 2014;9(1):349-372. doi:10.1146/annurev-pathol-012513-104656
2. Farrell PJ. Epstein–Barr Virus and Cancer. *Annu Rev Pathol: Mech Dis*. 2019;14(1):29-53. doi:10.1146/annurev-pathmechdis-012418-013023
3. Martel C de, Georges D, Bray F, Ferlay J, Clifford GM. Global burden of cancer attributable to infections in 2018: a worldwide incidence analysis. *Lancet Glob Heal*. 2020;8(2):e180-e190. doi:10.1016/s2214-109x(19)30488-7
4. Shannon-Lowe C, Rickinson A. The Global Landscape of EBV-Associated Tumors. *Front Oncol*. 2019;9:713. doi:10.3389/fonc.2019.00713
5. Pattengale P, Smith R, Gerber P. SELECTIVE TRANSFORMATION OF B LYMPHOCYTES BY E.B. VIRUS. *Lancet*. 1973;302(7820):93-94. doi:10.1016/s0140-6736(73)93286-8
6. Babcock GJ, Decker LL, Volk M, Thorley-Lawson DA. EBV Persistence in Memory B Cells In Vivo. *Immunity*. 1998;9(3):395-404. doi:10.1016/s1074-7613(00)80622-6
7. Thorley-Lawson DA. Epstein Barr Virus Volume 1, One Herpes Virus: Many Diseases. *Curr Top Microbiol Immunol*. 2015;390(Pt 1):151-209. doi:10.1007/978-3-319-22822-8_8
8. Bu GL, Xie C, Kang YF, Zeng MS, Sun C. How EBV Infects: The Tropism and Underlying Molecular Mechanism for Viral Infection. *Viruses*. 2022;14(11):2372. doi:10.3390/v14112372
9. Tanner J, Weis J, Fearon D, Whang Y, Kieff E. Epstein-barr virus gp350/220 binding to the B lymphocyte C3d receptor mediates adsorption, capping, and endocytosis. *Cell*. 1987;50(2):203-213. doi:10.1016/0092-8674(87)90216-9
10. Ogembo JG, Kannan L, Ghiran I, et al. Human Complement Receptor Type 1/CD35 Is an Epstein-Barr Virus Receptor. *Cell Rep*. 2013;3(2):371-385. doi:10.1016/j.celrep.2013.01.023
11. Chesnokova LS, Hutt-Fletcher LM. Fusion of Epstein-Barr Virus with Epithelial Cells Can Be Triggered by αvβ5 in Addition to αvβ6 and αvβ8, and Integrin Binding Triggers a Conformational Change in Glycoproteins gHgL. *J Virol*. 2011;85(24):13214-13223. doi:10.1128/jvi.05580-11
12. Wang HB, Zhang H, Zhang JP, et al. Neuropilin 1 is an entry factor that promotes EBV infection of nasopharyngeal epithelial cells. *Nat Commun*. 2015;6(1):6240. doi:10.1038/ncomms7240
13. Li Y, Zhang H, Sun C, et al. R9AP is a common receptor for EBV infection in epithelial cells and B cells. *Nature*. 2025;644(8075):205-213. doi:10.1038/s41586-025-09166-w
14. Li Q, Spriggs MK, Kovats S, et al. Epstein-Barr virus uses HLA class II as a cofactor for infection of B lymphocytes. *J Virol*. 1997;71(6):4657-4662. doi:10.1128/jvi.71.6.4657-4662.1997
15. Münz C. Latency and lytic replication in Epstein–Barr virus-associated oncogenesis. *Nat Rev Microbiol*. 2019;17(11):691-700. doi:10.1038/s41579-019-0249-7
16. Chamuleau MED, Stenner F, Chitu DA, et al. R-CODOX-M/R-IVAC versus DA-EPOCH-R in patients with newly diagnosed Burkitt lymphoma (HOVON/SAKK): final results of a multicentre, phase 3, open-label, randomised trial. *Lancet Haematol*. 2023;10(12):e966-e975. doi:10.1016/s2352-3026(23)00279-x
17. Storek J, Lindsay J. Rituximab for posttransplant lymphoproliferative disorder – therapeutic, preemptive, or prophylactic? *Bone Marrow Transplant*. 2024;59(1):6-11. doi:10.1038/s41409-023-02155-5

18. Diamantopoulos PT, Polonyfi K, Sofotasiou M, et al. Rituximab in the treatment of EBV-positive low grade B-cell lymphoma. *Anticancer Res*. 2013;33(12):5693-5698.
19. Liu L, Liu Q, Feng S. Management of Epstein–Barr virus-related post-transplant lymphoproliferative disorder after allogeneic hematopoietic stem cell transplantation. *Ther Adv Hematol*. 2020;11:2040620720910964. doi:10.1177/2040620720910964
20. Socié G, Barba P, Barlev A, et al. Outcomes for patients with EBV-positive PTLD post-allogeneic HCT after failure of rituximab-containing therapy. *Bone Marrow Transplant*. 2024;59(1):52-58. doi:10.1038/s41409-023-02127-9
21. Donk NWCJ van de, Zweegman S. T-cell-engaging bispecific antibodies in cancer. *Lancet*. 2023;402(10396):142-158. doi:10.1016/s0140-6736(23)00521-4
22. Jachimowicz RD, Borchmann S, Rothe A. Multi-Specific Antibodies for Cancer Immunotherapy. *BioDrugs*. 2014;28(4):331-343. doi:10.1007/s40259-014-0091-4
23. Gall JM, Davol PA, Grabert RC, Deaver M, Lum LG. T cells armed with anti-CD3 × anti-CD20 bispecific antibody enhance killing of $CD20^+$ malignant B cells and bypass complement-mediated rituximab resistance in vitro. *Exp Hematol*. 2005;33(4):452-459. doi:10.1016/j.exphem.2005.01.007
24. Ridgway JBB, Presta LG, Carter P. 'Knobs-into-holes' engineering of antibody CH3 domains for heavy chain heterodimerization. *Protein Eng, Des Sel*. 1996;9(7):617-621. doi:10.1093/protein/9.7.617
25. Patel RK, Jaszczak RG, Im K, et al. Cyclone: an accessible pipeline to analyze, evaluate, and optimize multiparametric cytometry data. *Front Immunol*. 2023;14:1167241. doi:10.3389/fimmu.2023.1167241
26. Strowig T, Gurer C, Ploss A, et al. Priming of protective T cell responses against virus-induced tumors in mice with human immune system components. *J Exp Med*. 2009;206(6):1423-1434. doi:10.1084/jem.20081720
27. Murer A, McHugh D, Caduff N, et al. EBV persistence without its EBNA3A and 3C oncogenes in vivo. *PLoS Pathog*. 2018;14(4):e1007039. doi:10.1371/journal.ppat.1007039
28. Lanzavecchia A, Sallusto F. Human B cell memory. *Curr Opin Immunol*. 2009;21(3):298-304. doi:10.1016/j.coi.2009.05.019
29. Shimabukuro-Vornhagen A, Gödel P, Subklewe M, et al. Cytokine release syndrome. *J Immunother Cancer*. 2018;6(1):56. doi:10.1186/s40425-018-0343-9
30. Leclercq-Cohen G, Steinhoff N, Albertí-Servera L, et al. Dissecting the mechanisms underlying the Cytokine Release Syndrome (CRS) mediated by T Cell Bispecific Antibodies. *Clin Cancer Res*. 2023;29(21):4449-4463. doi:10.1158/1078-0432.ccr-22-3667
31. Chatterjee B, Deng Y, Holler A, et al. $CD8^+$ T cells retain protective functions despite sustained inhibitory receptor expression during Epstein-Barr virus infection in vivo. *Plos Pathog*. 2019;15(5):e1007748. doi:10.1371/journal.ppat.1007748
32. Li J, Piskol R, Ybarra R, et al. CD3 bispecific antibody–induced cytokine release is dispensable for cytotoxic T cell activity. *Sci Transl Med*. 2019;11(508). doi:10.1126/scitranslmed.aax8861
33. Bröske AME, Korfi K, Belousov A, et al. Pharmacodynamics and molecular correlates of response to glofitamab in relapsed/refractory non-Hodgkin lymphoma. *Blood Adv*. 2022;6(3):1025-1037. doi:10.1182/bloodadvances.2021005954
34. Piccione EC, Belousov A, Hamidi H, et al. P1210: IMMUNE CORRELATES OF RESPONSE TO GLOFITAMAB: BIOMARKER FINDINGS FROM A PIVOTAL PHASE II EXPANSION STUDY IN PATIENTS WITH RELAPSED OR REFRACTORY (R/R) DIFFUSE LARGE B-CELL LYMPHOMA

(DLBCL). *HemaSphere*. 2022;6(Suppl):1096-1097. doi:10.1097/01.hs9.0000847704.12245.1f

35. Ramos E, Pollinger H, Stegall M, Gloor J, Dogan A, Grande J. The Effect of Desensitization Protocols on Human Splenic B-Cell Populations In Vivo. *Am J Transplant*. 2007;7(2):402-407. doi:10.1111/j.1600-6143.2006.01632.x
36. Audia S, Samson M, Guy J, et al. Immunologic effects of rituximab on the human spleen in immune thrombocytopenia. *Blood*. 2011;118(16):4394-4400. doi:10.1182/blood-2011-03-344051
37. Rehnberg M, Amu S, Tarkowski A, Bokarewa MI, Brisslert M. Short- and long-term effects of anti-CD20 treatment on B cell ontogeny in bone marrow of patients with rheumatoid arthritis. *Arthritis Res Ther*. 2009;11(4):R123. doi:10.1186/ar2789
38. Genberg H, Hansson A, Wernerson A, Wennberg L, Tydén G. Pharmacodynamics of Rituximab in Kidney Allotransplantation. *Am J Transplant*. 2006;6(10):2418-2428. doi:10.1111/j.1600-6143.2006.01497.x
39. Läderach F, Piteros I, Fennell É, et al. EBV induces CNS homing of B cells attracting inflammatory T cells. *Nature*. 2025; 646(8083):171-179. doi:10.1038/s41586-025-09378-0
40. Kamburova EG, Koenen HJPM, Borgman KJE, Berge IJ ten, Joosten I, Hilbrands LB. A Single Dose of Rituximab Does Not Deplete B Cells in Secondary Lymphoid Organs but Alters Phenotype and Function. *Am J Transplant*. 2013;13(6):1503-1511. doi:10.1111/ajt.12220
41. Leandro MJ, Cooper N, Cambridge G, Ehrenstein MR, Edwards JCW. Bone marrow B-lineage cells in patients with rheumatoid arthritis following rituximab therapy. *Rheumatology*. 2007;46(1):29-36. doi:10.1093/rheumatology/kel148
42. Strowig T, Chijioke O, Carrega P, et al. Human NK cells of mice with reconstituted human immune system components require preactivation to acquire functional competence. *Blood*. 2010;116(20):4158-4167. doi:10.1182/blood-2010-02-270678
43. Verma MK, Clemens J, Burzenski L, et al. A novel hemolytic complement-sufficient NSG mouse model supports studies of complement-mediated antitumor activity in vivo. *J Immunol Methods*. 2017;446:47-53. doi:10.1016/j.jim.2017.03.021
44. Meixlsperger S, Leung CS, Rämer PC, et al. CD141^{+} dendritic cells produce prominent amounts of IFN-α after dsRNA recognition and can be targeted via DEC-205 in humanized mice. *Blood*. 2013;121(25):5034-5044. doi:10.1182/blood-2012-12-473413
45. Gujer C, Murer A, Müller A, et al. Plasmacytoid dendritic cells respond to Epstein-Barr virus infection with a distinct type I interferon subtype profile. *Blood Adv*. 2019;3(7):1129-1144. doi:10.1182/bloodadvances.2018025536
46. Chijioke O, Müller A, Feederle R, et al. Human Natural Killer Cells Prevent Infectious Mononucleosis Features by Targeting Lytic Epstein-Barr Virus Infection. *Cell Reports*. 2013;5(6):1489-1498. doi:10.1016/j.celrep.2013.11.041
47. Pavlasova G, Mraz M. The regulation and function of CD20: an “enigma” of B-cell biology and targeted therapy. *Haematologica*. 2020;105(6):1494-1506. doi:10.3324/haematol.2019.243543
48. Braun A, Gouni S, Pulles A, Strati P, Minnema MC, Budde LE. Bispecific Antibody Use in Patients With Lymphoma and Multiple Myeloma. *Am Soc Clin Oncol Educ Book*. 2024;44(3):e433516. doi:10.1200/edbk_433516
49. Lancman G, Sastow DL, Cho HJ, et al. Bispecific Antibodies in Multiple Myeloma: Present and Future. *Blood Cancer Discov*. 2021;2(5):423-433. doi:10.1158/2643-3230.bcd-21-0028

50. Hansson M, Falk K, Ernberg I. Epstein-Barr virus transformation of human pre-B cells. *J Exp Med*. 1983;158(2):616-622. doi:10.1084/jem.158.2.616
51. Ernberg I, Falk K, Hansson M. Progenitor and pre-B lymphocytes transformed by Epstein-Barr virus. *Int J Cancer*. 1987;39(2):190-197. doi:10.1002/ijc.2910390212
52. Hui MF, Lam P, Dosch HM. Properties and heterogeneity of human fetal pre-B cells transformed by EBV. *J Immunol*. 1989;143(8):2470-2479. doi:10.4049/jimmunol.143.8.2470
53. Bandyopadhyay S, Duffy MP, Ahn KJ, et al. Mapping the cellular biogeography of human bone marrow niches using single-cell transcriptomics and proteomic imaging. *Cell*. 2024;187(12):3120-3140.e29. doi:10.1016/j.cell.2024.04.013
54. Crombie JL, Graff T, Falchi L, et al. Consensus recommendations on the management of toxicity associated with CD3×CD20 bispecific antibody therapy. *Blood*. 2024;143(16):1565-1575. doi:10.1182/blood.2023022432
55. Bacac M, Colombetti S, Herter S, et al. CD20-TCB with Obinutuzumab Pretreatment as Next-Generation Treatment of Hematologic Malignancies. *Clin Cancer Res*. 2018;24(19):4785-4797. doi:10.1158/1078-0432.ccr-18-0455
56. Wat J, Barmettler S. Hypogammaglobulinemia After Chimeric Antigen Receptor (CAR) T-Cell Therapy: Characteristics, Management, and Future Directions. *J Allergy Clin Immunol: Pract*. 2022;10(2):460-466. doi:10.1016/j.jaip.2021.10.037
57. Chen S, An L, Han J, et al. Successful Blinatumomab treatment in an allogeneic hematopoietic stem cell transplant recipient with EBV-related post-transplant lymphoproliferative disorder: A case report and literature review. *Transpl Immunol*. 2023;80:101895. doi:10.1016/j.trim.2023.101895
58. Janardan S, Watkins B, Williams KM, et al. Blinatumomab Induces Complete Response in Refractory PTLD after Hematopoietic Cell Transplantation. *Blood Adv*. 2022;6(10):3058-3061. doi:10.1182/bloodadvances.2021006535
59. Tsai MH, Raykova A, Klinke O, et al. Spontaneous Lytic Replication and Epitheliotropism Define an Epstein-Barr Virus Strain Found in Carcinomas. *Cell Rep*. 2013;5(2):458-470. doi:10.1016/j.celrep.2013.09.012
60. Feederle R, Neuhierl B, Bannert H, Geletneky K, Shannon-Lowe C, Delecluse H. Epstein-Barr virus B95.8 produced in 293 cells shows marked tropism for differentiated primary epithelial cells and reveals interindividual variation in susceptibility to viral infection. *Int J Cancer*. 2007;121(3):588-594. doi:10.1002/ijc.22727
61. Delecluse HJ, Hilsendegen T, Pich D, Zeidler R, Hammerschmidt W. Propagation and recovery of intact, infectious Epstein–Barr virus from prokaryotic to human cells. *Proc Natl Acad Sci*. 1998;95(14):8245-8250. doi:10.1073/pnas.95.14.8245
62. Antsiferova O, Müller A, Rämer PC, et al. Adoptive Transfer of EBV Specific $CD8^+$ T Cell Clones Can Transiently Control EBV Infection in Humanized Mice. *Plos Pathog*. 2014;10(8):e1004333. doi:10.1371/journal.ppat.1004333
63. Song R, Bafit M, Tullett KM, et al. A Simple and Rapid Protocol for the Isolation of Murine Bone Marrow Suitable for the Differentiation of Dendritic Cells. *Methods Protoc*. 2024;7(2):20. doi:10.3390/mps7020020
64. Mietz J, Kaulfuss M, Egli L, Opitz L, Münz C, Chijioke O. Human effector $CD8^+$ T cells with an activated and exhausted-like phenotype control tumour growth in vivo in a humanized tumour model. *eBioMedicine*. 2024;106:105240. doi:10.1016/j.ebiom.2024.105240
65. Amezquita RA, Lun ATL, Becht E, et al. Orchestrating single-cell analysis with Bioconductor. *Nat Methods*. 2020;17(2):137-145. doi:10.1038/s41592-019-0654-x

606 66. Bunis DG, Andrews J, Fragiadakis GK, Burt TD, Sirota M. dittoSeq: universal user-friendly
607 single-cell and bulk RNA sequencing visualization toolkit. *Bioinformatics*. 2020;36(22-
608 23):5535-5536. doi:10.1093/bioinformatics/btaa1011
609 67. McHugh D, Caduff N, Barros MHM, et al. Persistent KSHV Infection Increases EBV-
610 Associated Tumor Formation In Vivo via Enhanced EBV Lytic Gene Expression. *Cell Host*
611 *Microbe*. 2017;22(1):61-73.e7. doi:10.1016/j.chom.2017.06.009
612 68. Caduff N, McHugh D, Murer A, et al. Immunosuppressive FK506 treatment leads to more
613 frequent EBV-associated lymphoproliferative disease in humanized mice. *Plos Pathog*.
614 2020;16(4):e1008477. doi:10.1371/journal.ppat.1008477
615 69. Bell AI, Groves K, Kelly GL, et al. Analysis of Epstein–Barr virus latent gene expression in
616 endemic Burkitt's lymphoma and nasopharyngeal carcinoma tumour cells by using
617 quantitative real-time PCR assays. *J Gen Virol*. 2006;87(10):2885-2890.
618 doi:10.1099/vir.0.81906-0

619

Figure Legends

Figure 1: CD20 bispecific T cell engager-mediated B cell depletion prevents systemic virus spread and EBV-induced tumor formation. **(A)** Experiment set-up: Three to six months old humanized mice were intraperitoneally (ip) infected with 10^5 Raji infecting units (RIU) of EBV or mock infected with PBS. Starting from week two, mice received weekly doses of the vehicle, PBS, an isotype control (100µg/kg) or the bispecific TCE (100µg/kg). Blood was taken weekly until the mice were sacrificed five weeks post infection. In week two, the blood was collected six hours after the first antibody injection. **(B)** Number of $CD19^+$ and $CD20^+$ cells per mL tail vein blood over time as measured by flow cytometry. Graphs show mean +/- SD of four (TCE, Isotype) three (PBS) or two (Vehicle) independently performed experiments with n= 9 (PBS), n=17-21 (Isotype), n=17-24 (TCE), n=7-12 (Vehicle). Linear mixed model fit by REML taking the experiment into account as a random effect with Tukey post-hoc test for multiple comparisons. Reported p-values are adjusted with the Holm method. **(C)** Total numbers of $CD20^+$ or $CD19^+$ cells per spleen and bone marrow (BM) as measured by flow cytometry at experiment termination. Graphs show mean +/- SD of four (TCE, Isotype), three (PBS) or two (Vehicle) independently performed experiments with n=11 (Vehicle), n=22 (Spleen Isotype), n=21 (BM Isotype), n=20 (TCE), n=9 (PBS). Linear mixed model fit by REML taking the experiment into account as a random effect with Tukey post-hoc test for multiple comparisons. Reported p-values are adjusted with the Holm method. **(D)** EBV loads in peripheral blood over time of infected humanized mice as measured by qPCR on BamHI-W repeat regions of EBV DNA. Graph shows mean +/- SD of two independently performed experiments with n=12 (Vehicle weeks 3-4), n=11 (Vehicle week 5), n=9 (Isotype week 3), n=10 (Isotype week 4-5), n=12 (TCE week 3), n=11 (TCE weeks 4 and 5). Linear mixed model fit by REML of $\log_{10}$ transformed EBV loads taking the experiment into account as a random effect with Tukey post-hoc test for multiple comparisons. Reported p-values are adjusted with the Holm method. **(E)** EBV loads in the spleen of infected humanized mice as measured by qPCR on BamHI-W repeat regions of EBV DNA. Graph shows mean +/- SD of two independently performed experiments with n=11 (Vehicle), n=10 (Isotype), n=11 (TCE). Linear mixed model fit by REML of $\log_{10}$ transformed EBV loads taking the experiment into account as a random effect with Tukey post-hoc test for multiple comparisons. Reported p-values are adjusted with the Holm method. **(F)** Tumor incidence in EBV infected humanized mice treated with vehicle, isotype or TCE five weeks after infection. Graph shows proportion of animals with or without macroscopically visible tumors of two independently performed experiments with n=11 (Vehicle), n=11 (Isotype), n=12 (TCE). Distributions per category are indicated in the bar graph. Fisher's exact test, p=0.0006. **(A - F)** Significance: * $p \leq 0.05$, ** $p \leq 0.01$, *** $p \leq 0.001$. Statistical analyses were carried out using R Statistical Software (R Core Team 2021) with lme4 (v1.1, Bates 2015) and multcomp package (v1.4, Hothorn 2008) or GraphPad Prism v10.2.

Figure 2: T cells expand and differentiate after CD20 TCE injection. **(A)** Weight measurements normalized to the weight at baseline are given over the course of the experiment for each experimental group. Arrows indicate the days of antibody injection; the dashed line indicates the threshold for euthanizing the animals based on their weight loss according to the humane endpoints defined for the study. Graph shows mean+/- SEM of one (PBS) or two independent experiments (Vehicle, Isotype, TCE) with n=6-11 (Vehicle), n=7-11 (Isotype), n=8-14 (TCE), n=3 (PBS). **(B)** Plasma cytokine concentrations in EBV infected humanized mice 6 hours after the first injection of vehicle, isotype or TCE. Graphs show mean +/- SD of two independently performed experiments with n=4 (Vehicle IL-1β), n=6 (Vehicle IL-4), n=7 (Vehicle rest), n=8 (Isotype IL-1B), n=11 (Isotype rest), n=8 (TCE IL-1β), n=23 (TCE IFNγ), n=24 (TCE rest). One-way ANOVA with Tukey's post-hoc test for multiple comparisons. **(C)** Total number of $CD3^+$ cells per mL blood plotted per week and experimental group. Graph shows median +/- SD of four (TCE, Isotype), three (PBS) or two (Vehicle) independently performed experiments with n=7-12 (Vehicle), n=16-21 (Isotype), n=19-25 (TCE), n=9 (PBS). Linear mixed model fit by REML taking the experiment into account as a random effect with Tukey post-hoc test for multiple comparisons. Reported p-values are adjusted with the Holm method. **(D)** Mean proportion of the four T cell activation states plotted over time and per experimental group. Graph shows data of three (TCE n=19, Isotype n=18, PBS n=9) or one (Vehicle n=6) independently performed experiments. **(E)** Frequency of $HLA\text{-}DR^-$ $PD1^-$ $CD3^+$ T cells plotted over time and per experimental

group. Graph shows boxplots and individual values of three (TCE, Isotype, PBS) or one (Vehicle) independently performed experiments with n=4-6 (Vehicle), n=16-18 (Isotype), n=17-19 (TCE), n=8-9 (PBS). Linear mixed model fit by REML taking the experiment into account as a random effect with Tukey post-hoc test for multiple comparisons. Reported p-values are adjusted with the Holm method. **(F)** Mean proportion of the four T cell differentiation stages plotted over time and per experimental group. Graph shows data of four (TCE n=25, Isotype n=22), three (PBS=9) or two (Vehicle n=11) independently performed experiments. **(G)** Frequency of Temra ($CD45RA^+$ $CCR7^-$) $CD3^+$ T cells plotted over time and per experimental group. Graph shows mean frequency of four (TCE, Isotype), three (PBS) or two (Vehicle) independently performed experiments with n=4-11 (Vehicle), n=18-22 (Isotype), n=17-25 (TCE), n=8-9 (PBS). Linear mixed model fit by REML taking the experiment into account as a random effect with Tukey post-hoc test for multiple comparisons. Reported p-values are adjusted with the Holm method. **(A - G)** Significance: * $p \leq 0.05$, ** $p \leq 0.01$, *** $p \leq 0.001$. Statistical analyses were carried out using R Statistical Software (R Core Team 2021) with lme4 (v1.1, Bates 2015) and multcomp package (v1.4, Hothorn 2008) or GraphPad Prism v10.2

Figure 3: CD20 TCE treatment prevents EBV-induced lymphomagenesis more efficiently than the CD20 monospecific antibody Rituximab. **(A)** Experiment set-up: Three to six months old, humanized mice were intraperitoneally (ip) infected with 10^5 Raji infecting units (RIU) of EBV or mock infected with PBS. Starting from two weeks post infection, mice received weekly doses of Rituximab, PBS, the TCE (100µg/kg) or an isotype control (100µg/kg). Blood was taken weekly until the mice were sacrificed five weeks post infection. In week two, the blood was collected six hours after the first antibody injection. **(B)** Frequency of $CD20^+$ or $CD19^+$ cells within the human $CD45^+$ immune cell compartment over time and per experimental group measured by flow cytometry in tail vein blood. Graphs show boxplots and individual values of two independently performed experiments with n=9-11 (Isotype), n=12 (Rituximab), n=11 (TCE). Linear mixed model fit by REML taking the experiment into account as a random effect with Tukey post-hoc test for multiple comparisons. Reported p-values are adjusted with the Holm method. **(C)** Frequency of $CD20^+$ or $CD19^+$ cells within the human $CD45^+$ immune cell compartment per spleen and bone marrow (BM) measured by flow cytometry at experiment termination. Graphs show mean +/- SD of two independently performed experiments with n=11 (Isotype spleen), n=12 (Rituximab), n=10 (TCE), n=10 (Isotype BM). Linear mixed model fit by REML taking the experiment into account as a random effect with Tukey post-hoc test for multiple comparisons. Reported p-values are adjusted with the Holm method. **(D)** EBV loads in peripheral blood over time of infected humanized mice as measured by qPCR on BamHI-W repeat regions of EBV DNA at experiment endpoint. Graph shows geometric mean +/- geometric SD of two independently performed experiments with n=5-7 (Isotype), n=6-7 (TCE), n=6-7 (Rituximab), n=6 (PBS). Linear mixed model fit by REML of $\log_{10}$ transformed EBV loads taking the experiment into account as a random effect with Tukey post-hoc test for multiple comparisons. Reported p-values are adjusted with the Holm method. **(E)** EBV loads in the spleen and bone marrow (BM) as measured by qPCR on BamHI-W repeat regions of EBV DNA at experiment endpoint. Graph shows geometric mean +/- geometric SD of two independently performed experiments with n=9 (spleen TCE), n=11 (BM TCE), n=12 (Rituximab), n=11 (spleen Isotype), n=10 (BM Isotype), n=6 (PBS). Linear mixed model fit by REML of $\log_{10}$ transformed EBV loads taking the experiment into account as a random effect with Tukey post-hoc test for multiple comparisons. Reported p-values are adjusted with the Holm method. **(F)** Tumor incidence in EBV infected humanized mice treated with Rituximab, isotype or TCE five weeks after infection. Graph shows proportion of animals with or without macroscopically visible tumors of two independently performed experiments with n=13 (Rituximab), n=12 (Isotype), n=12 (TCE). Distributions per category are indicated in the bar graph. Fisher's exact test, p=0.0003. **(A - F)** Significance: * $p \leq 0.05$, ** $p \leq 0.01$, *** $p \leq 0.001$. Statistical analyses were carried out using R Statistical Software (R Core Team 2021) with lme4 (v1.1, Bates 2015) and multcomp package (v1.4, Hothorn 2008) or GraphPad Prism v10.2.

Figure 4: CD20 TCE treatment depletes precursor B cells in the bone marrow. **(A)** UMAP of $CD19^+$ and/or $CD20^+$ B cells derived from bone marrow, spleen and heart puncture blood of EBV or PBS mock infected humanized mice treated with the TCE, an isotype control, Rituximab or PBS. Different B cell clusters are colored. **(B)** Heatmap

of mean z-score scaled expression values of each marker per cluster. **(C)** UMAP of $CD19^+$ and/or $CD20^+$ B cells derived from bone marrow, spleen and heart puncture blood of EBV or PBS mock infected humanized mice plotted for each experimental group. TCE, Isotype and Rituximab treated animals were infected with EBV, whereas PBS treated animals were only mock infected with PBS. **(D)** Stacked bar plots showing the percentage of cells per experimental group and organ belonging to the respective cluster. There is a significant relationship between the cluster and the experimental group in the Bone Marrow ($X2(15,288250)=37567$, $P=0$, $\omega=0.361$), the spleen ($X2(15,304644)=59209$, $P=0$, $\omega=0.4409$), and in the blood ($X2(15,96782)=23149$, $P=0$, $\omega=0.49$). Pearson's Chi-squared test for count data. **(E)** Frequencies of different B cell subsets within the $CD19^+$ and/or $CD20^+$ B cell population in each organ (BM = bone marrow, spleen, HP = heart puncture blood) plotted per experimental group. Graphs show boxplots and individual values of two independently performed experiments with n=10 (Isotype BM), n=9 (Isotype HP), n=11 (Isotype spleen), n=6 (PBS), n=12 (Rituximab), n=10 (TCE). Linear mixed model fit by REML taking the experiment into account as a random effect with Tukey post-hoc test for multiple comparisons. Reported p-values are adjusted with the Holm method. **(A - E)** Significance: * $p \leq 0.05$, ** $p \leq 0.01$, *** $p \leq 0.001$. Statistical analyses were carried out using R Statistical Software (R Core Team 2021) with lme4 (v1.1, Bates 2015), multcomp package (v1.4, Hothorn 2008), gmodels package (v2.19, Warnes 2024) and rcompanion package (v2.4, Mangiafico 2024).

Figure 5: Depletion of precursor B cells protects from systemic virus spread. **(A)** UMAP of $CD19^+$ and/or $CD20^+$ B cells derived from bone marrow, spleen and heart puncture blood of EBV infected, TCE treated humanized mice plotted for animals with detectable BamHI-W repeat regions of EBV DNA (black) or without detectable BamHI-W repeat regions of EBV DNA (blue) in any organ as measured by qPCR. **(B)** Frequency of $CD24^+$ B cells within the $CD19^+$ and/or $CD20^+$ B cell population in each organ (BM = bone marrow, spleen, heart puncture blood) of EBV infected, TCE treated humanized mice plotted for animals with detectable BamHI-W repeat regions of EBV DNA (black) or without detectable BamHI-W repeat regions of EBV DNA (blue). Graph shows boxplot and individual values of 2 independently performed experiments with n=6 (no detectable BamHI-W, BM and spleen), n=5 (no detectable BamHI-W, HP), n=4 (detectable BamHI-W, BM and spleen), n=5 (detectable BamHI-W, HP). Linear mixed model fit by REML taking the experiment into account as a random effect with Tukey post-hoc test for multiple comparisons. Reported p-values are adjusted with the Holm method. **(C)** Experimental set-up: splenocytes and bone marrow cells were isolated from humanized mice, sorted for $CD24^+$ and $CD24^-$ cells and infected with EBV (MOI=1). Three days after infection, RNA was isolated from the cells and rt-qPCR was performed for EBNA2, LMP1, LMP2A and BZLF1. Alternatively, cells were co-stained three days after infection for EBNA1 and CD24 and analysed via ImageStream. **(D)** Relative gene expression of EBNA2, LMP1, LMP2a and BZLF1 normalized to GAPDH in $CD24^+$ (spleen, BM) or $CD24^-$ (spleen) B cells three days after infection with EBV. Graph shows mean ± SD. Each dot corresponds to cells isolated from a different humanized mouse. **(E)** Concatenated fluorescent intensity histograms of CD21 and CD35 expression in $CD24^+$ and $CD24^-$ cells derived from BM or spleen of three humanized mice and in positive control cells (Raji) and negative control cells (NALM6). **(F)** Frequency of $CD24^+$ bone marrow or spleen cells expressing nuclear EBNA1 three days after infection with EBV, or in uninfected control cells. To rule out a virus-specific effect, both rB95-8 and rM81 EBV strains were used. Graph shows mean ± SD. Symbols indicate the experiment with cells from HPC-reconstituted NSG mice (circles) or A2DR2 mice (star), the latter being the mouse background used for the scRNA-seq dataset reanalyzed in Fig. S8B. **(G)** Representative images of uninfected, B95-8-infected or M81-infected cells obtained by ImageStream analysis. EBNA1 and CD24 co-staining is detectable in infected cells but absent in uninfected controls. **(H)** Experimental set-up: bone marrow cells were isolated from EBV-infected humanized mice, sorted for $CD3^+$, $CD3^-CD19^-CD20^-$, $CD24^+$ B cells and $CD24^-$ B cells. DNA was isolated from FACS-sorted and total unsorted cells and BamHI-W repeat regions of EBV DNA were detected by qPCR. **(I)** Relative quantification of BamHI-W repeat regions of EBV DNA : GAPDH-normalized fold-change of BamHI-W repeat regions of EBV DNA within the sorted populations relative to the unsorted total fraction. Graph shows mean +/- SD of three independently performed experiments, n=7. Each dot corresponds to cells isolated from a different humanized mouse. Symbols correspond to three different HPC donors used to reconstitute the humanized mice (star: NSG, rest: NFA2) in the three

765 independent experiments. Mice without detectable viral loads in the sorted population were set to 2^{-10} indicated
766 by the dashed line. One-way ANOVA with Tukey's post-hoc test for multiple comparisons **(A - E)** Significance: * p
767 ≤ 0.05, ** p ≤ 0.01, *** p ≤ 0.001. Statistical analyses were carried out using R Statistical Software (R Core Team
768 2021) with lme4 (v1.1, Bates 2015), multcomp package (v1.4, Hothorn 2008), gmodels package (v2.19, Warnes
769 2024) and rcompanion package (v2.4, Mangiafico 2024) or GraphPad Prism v10.2.

770

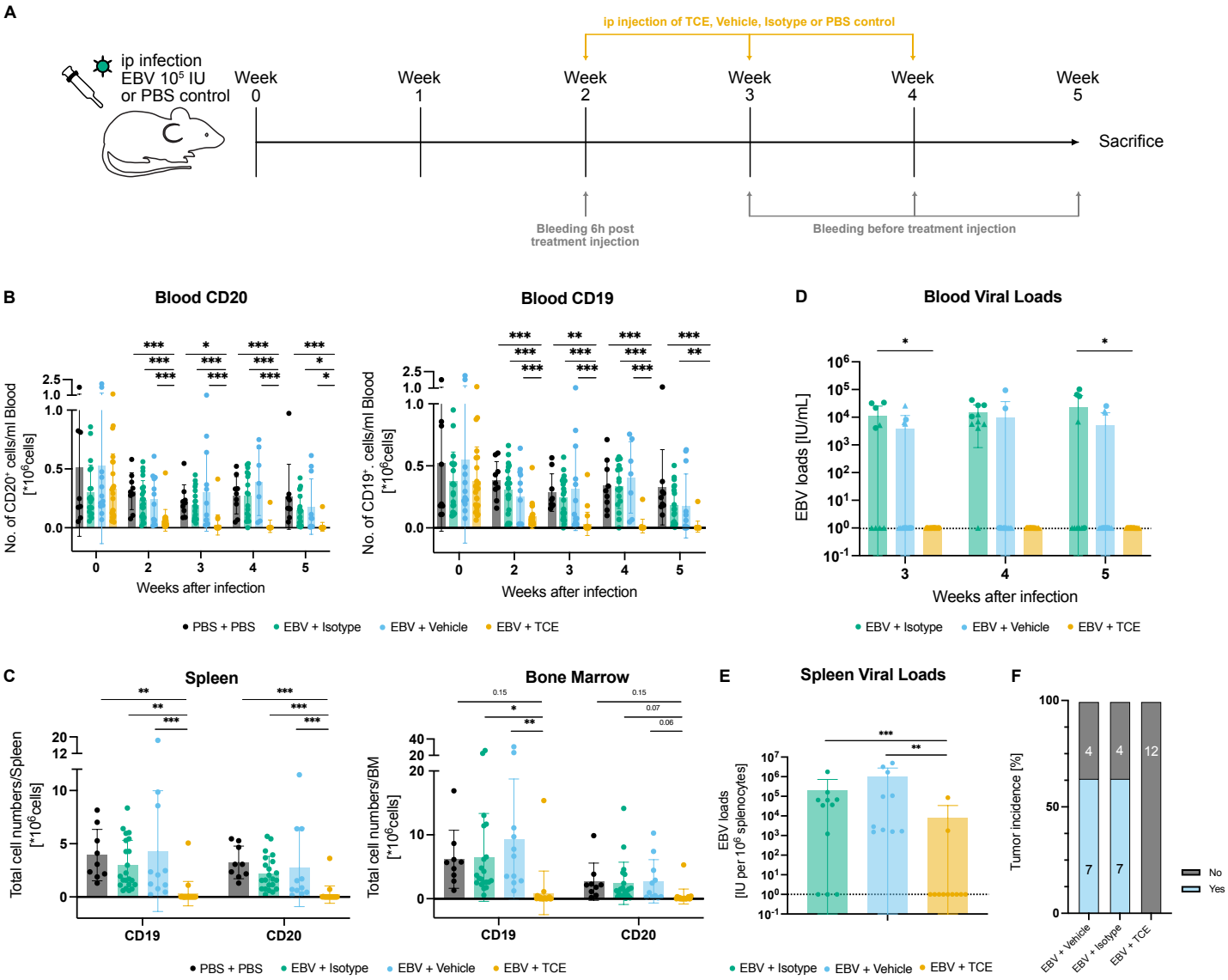

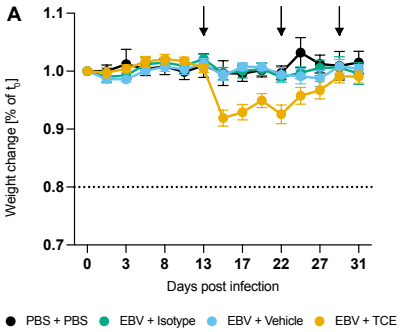

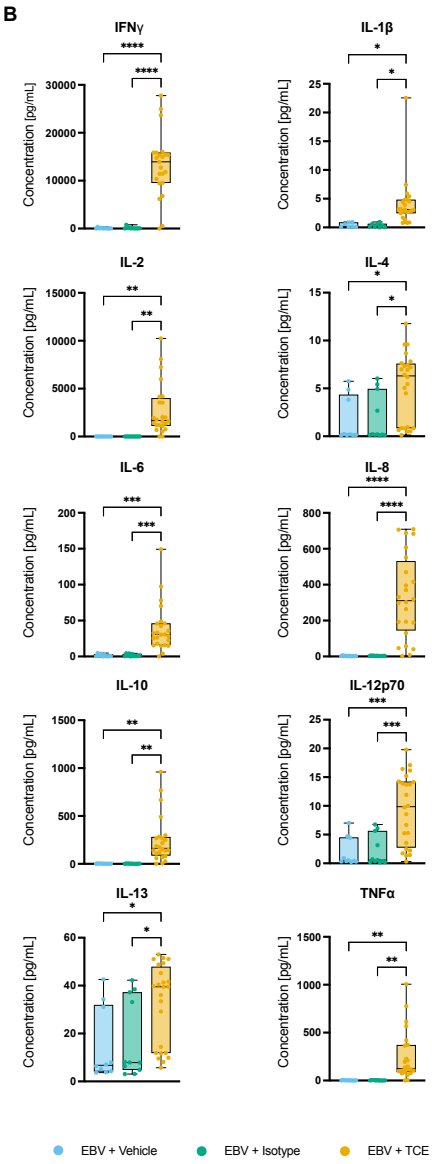

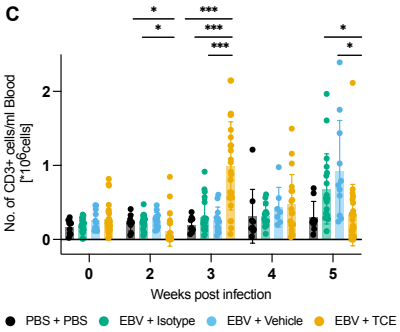

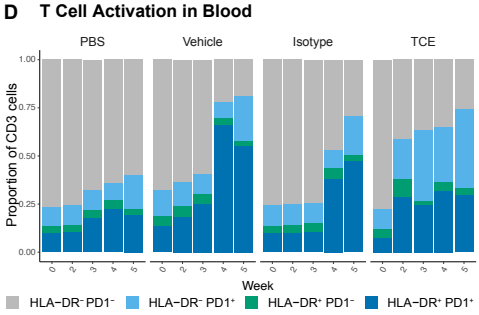

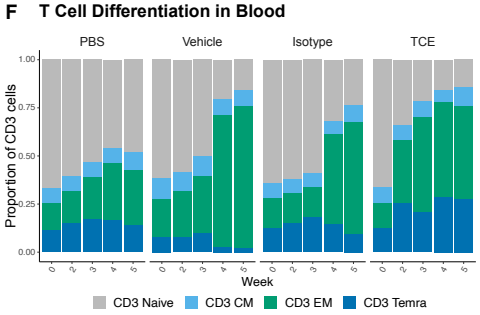

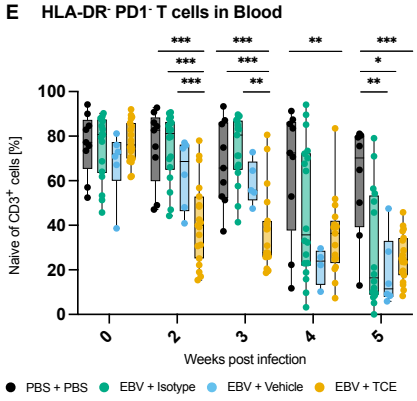

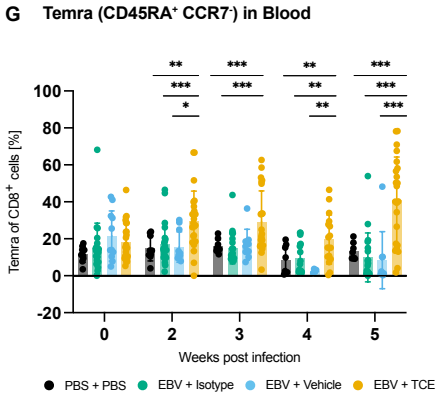

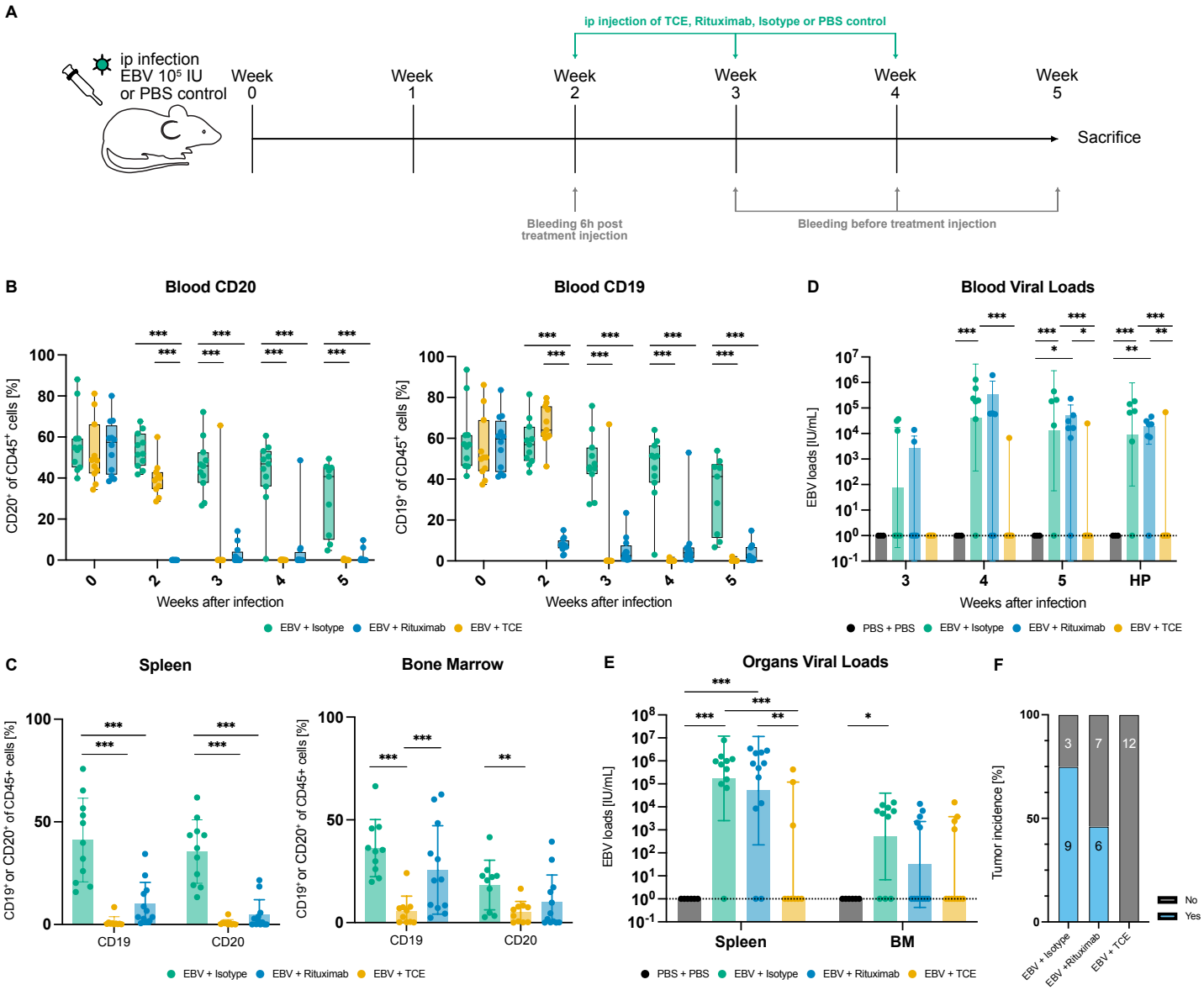

Figure 4

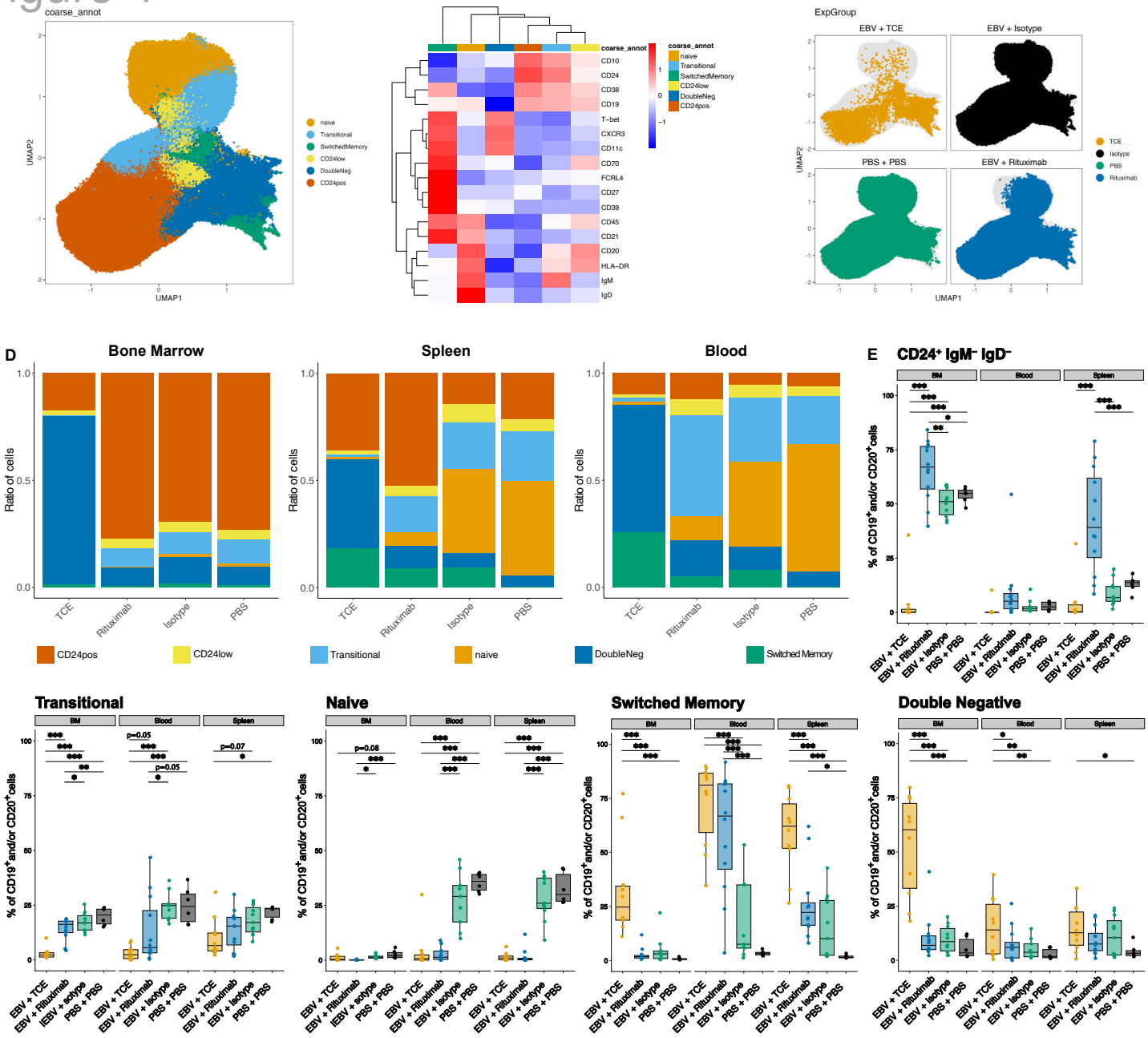

Figure 5